RSC Advances

PAPER

View Article Online
View Journal | View Issue

Cite this: *RSC Adv.*, 2019, **9**, 704

Effect of tourmaline nanoparticles on the anticoagulation and cytotoxicity of poly(L-lactide-*co*-caprolactone) electrospun fibrous membranes†

Tianyu Zhao,[abc] Hong Zhang, *[abc] Pan Li[abc] and Jinsheng Liang*[abc]

Tourmaline nanoparticles (TM NPs) were well dispersed in poly(L-lactide-*co*-caprolactone) (PLCL) fibers *via* electrospinning without a dispersant. Through the modification of TM NPs, the hydrophilicity and anticoagulant property of the composite electrospun fibrous membranes were improved. Compared with the PLCL membranes, the curve of dynamic clotting time in contact with the composite TM NPs/PLCL membranes descended more slowly. Particularly, the coagulation time of 8 wt% TM NPs/PLCL membrane was longer than 70 min, which was 174% higher than that of the PLCL membrane. At the same time, the cell compatibility and mechanical properties of TM NPs/PLCL membranes were analyzed. The cytotoxicity test showed that the grade of 8 wt% TM NPs/PLCL membrane was 0. The stretching experiments showed that the tensile strength of 8 wt% TM NPs/PLCL membrane (6.71 ± 0.30 MPa) was 267.33% higher than that of the PLCL membrane, and its elongation at break (141.83 ± 5.82%) was higher than the requirement of the coronary artery. These results indicated that the PLCL electrospun fibrous membranes modified with TM NPs have potential to be used in tissue engineering as small-caliber vascular grafts.

Received 16th September 2018
Accepted 4th December 2018

DOI: 10.1039/c8ra07700b

rsc.li/rsc-advances

Introduction

Regeneration of blood vessels by tissue engineering technology has been applied widely to treat vascular occlusion or injury.[1,2] However, the low-flow and high-shear in small-caliber blood vessels (diameter < 6 mm) is prone to postoperative thrombosis and intimal hyperplasia, and there are few successful cases for its reconstruction currently. When contacting the artificial vascular graft, the fibrin in blood is adsorbed on the graft surface and becomes the structural basis for thrombosis. Thus, the calcium ions promote adherence of erythrocytes and platelets by fibrin to form the thrombus. Therefore, improving the anticoagulant property is of critical importance in small-caliber vascular graft research.[3–7] In recent years, a series of biocompatible materials and modification methods have been studied to simulate the natural vessels.[8–19] For instance, hydrophilic natural proteins and polysaccharides, such as silk fibroin or chitosan, were introduced into artificial blood vessels to improve the anticoagulant property of the matrix materials.[9–11] The heparinization can introduce negative charges on the surfaces to inhibit the activity of thrombin.[12–14] The appropriate growth factors or miRNA are also chosen for the endothelialization of the lumen surface, but a short half-life limits their application.[16–19]

Tourmaline (TM) is a multi-element silicate mineral; the general chemical formula can be written as $XY_3Z_6Si_6O_{18}(BO_3)_3W_4$ (where X can be Na, Ca, K or vacancies; Y can be Mg^{2+}, Fe^{2+}, Mn^{2+}, Al^{3+}, Fe^{3+}, Mn^{3+}, Li^{+}; Z can be Al^{3+}, Fe^{3+}, Cr^{3+}, Mg^{2+}; W can be OH^{-}, F^{-}, O^{2-}). TM crystals are symmetric about the *c*-axis, and there is neither a symmetric surface nor a symmetric center in the direction of the vertical *c*-axis. Thus the high asymmetry causes many molecular vibrations inside the crystal, which endows tourmaline with many properties such as spontaneously polarizable, pyroelectric, piezoelectric and radiating in the far infrared region.[20,21] In our previous experiments, we found that tourmaline can regulate calcium salt deposition and slow down the crystal formation.[22] After immersion in the simulated body fluid with shaking, the increasing ratio of calcium deposition on composite membranes containing TM was lower than that of a pure polymer membrane, thereby it may be an effective mean for retarding coagulation.

The electrospun technology is a method of preparing fibrous membranes through the electrostatic breakdown of polymer solution in a high voltage electrostatic field.[23] The products of electrospun membranes have attracted wide attention because of their structure being similar to the extracellular matrices and

[a]Key Laboratory of Special Functional Materials for Ecological Environment and Information (Hebei University of Technology), Ministry of Education, Tianjin 300130, China. E-mail: zhanghong@hebut.edu.cn; liangjinsheng@hebut.edu.cn

[b]Institute of Power Source and Ecomaterials Science, Hebei University of Technology, Tianjin 300130, China

[c]Key Laboratory for New Type of Functional Materials in Hebei Province, Hebei University of Technology, Tianjin 300130, China

† Electronic supplementary information (ESI) available. See DOI: 10.1039/c8ra07700b

excellent mechanical properties for vascular grafts.[24] L. D. Tijing has obtained a dispersed homogeneous tourmaline/polyurethane antibacterial membrane with good mechanical properties by the electrospinning method.[25] However, a high content of Triton X-100 was added as a dispersant, which makes this membrane unsuitable for tissue engineering. Therefore, the preparation method needs improvement for small-caliber vascular grafts.

In this study, TM particles with an average diameter of 100 nm were obtained and dispersed into the biocompatible poly(L-lactide-*co*-caprolactone) (PLCL) matrix without a dispersant. The uniformly dispersed tourmaline nanoparticle/PLCL composite membranes were prepared by electrospinning. Subsequently, the anticoagulant properties of the composites were mainly studied, including their morphology characterization and hydrophilicity. In addition, the cytotoxicity and mechanical properties of the composites were also tested in order to prepare the scaffolds for vascular tissue engineering.

Experimental

Materials

The tourmaline ore is from Hebei Province of China. Poly(L-lactide-*co*-caprolactone) (PLCL) has a weight-average molecular weight of 20 000 and was purchased from Jinan Biotech Co., Ltd. Mouse fibroblasts (L929) were obtained from the cell bank of the Chinese Academy of Sciences. Dimethyl sulfoxide (DMSO) and 3-(4,5-dimethylthiazole-2)-2,5-diphenyltetrazolium bromide (MTT) were obtained from Sigma, USA. Calf serum, Los Angeles Park Memorial Institute 1640 (RPMI 1640) culture fluid was obtained from Gibco, USA. Dichloromethane (CH_2Cl_2, AR) and *N*,*N*-dimethylformamide (DMF, AR) were purchased from Tianjin Sailboat Chemical Reagent Technology Co., Ltd.

Characterization of tourmaline nanoparticles

The morphology of tourmaline nanoparticles (TM NPs) after ball milling was observed by a scanning electron microscope (SEM, NanoNova 450, FEI, USA). The crystal structure of TM NPs was detected by X-ray diffraction (XRD, D8 Advance, Bruker, Germany). At the same time, the TM particles were dispersed in an alcohol solution by ultrasonic agitation for 0.5 h and the zeta potential of the samples were tested using a Malvern Nano ZS90 (UK).

Preparation of TM NPs/PLCL composite membranes

For electrospinning, the PLCL solution was prepared in solvent A (CH_2Cl_2 : DMF = 7 : 3, v/v). For the mixed solution of TM NPs/PLCL system (containing 2 wt%, 4 wt%, 6 wt% or 8 wt% of TM NPs), PLCL was dissolved in 90% of the volume of solvent A, according to the above method. The remaining 10% solvent was ultrasonically mixed (SL-900DL, Nanjing Shunliu Instrument Co., Ltd. PRC) with TM NPs in PLCL solution to obtain a TM NPs suspension. After three hours of crushing, we tested the viscosity (DV-1, Brookfield, USA), conductivity (DDSJ-318, Shanghai INESA Scientific Instrument Co., Ltd. PRC) and surface tension (DCAT21, Data Physics, Germany) of the solutions. The electrospinning device consists of a high voltage power supply, a single channel injector and a radial receiver. The glass needle with the spinning solution is fixed on the single-channel syringe (78-9100c, Cole-Parmer, USA). During electrospinning, the voltage is 18 kV and the flow rate is 0.8 mL h^{-1}.

Morphology and structure observation

The surface morphology and elemental analysis of TM NPs/PLCL composite membranes was observed at an acceleration voltage of 15 kV using a scanning electron microscope (SEM, S4800, Hitachi, Japan). The internal structure of the composite membrane was observed by a transmission electron microscope (TEM, HT7700, Hitachi, Japan) at an acceleration voltage of 80 kV and a high resolution transmission electron microscope (HRTEM, Tecnai G2 F20, FEI, US). The infrared spectrometer (TENSOR II, Bruker, Germany) and differential scanning calorimeter (DSC, q20, TA, US) were used to investigate the properties of different membranes.

Contact angle

The static contact angle of the samples was tested by a video contact angle meter (OCA20, Data Physics, Germany).

Dynamic coagulation

5 mm × 5 mm square electrospun membranes (containing PLCL, 2 wt% TM NPs/PLCL, 4 wt% TM NPs/PLCL, 6 wt% TM NPs/PLCL, 8 wt% TM NPs/PLCL) were placed in an Erlenmeyer flask with a constant temperature water bath at 37 °C. Then, 0.25 mL of anticoagulated rabbit blood (3.8% sodium citrate: blood = 1 : 9, from the male New Zealand white rabbits supplied by Tianjin Institute of Medical and Pharmaceutical Sciences) was added in the membranes. After 10 min, 0.02 mL of $CaCl_2$ aqueous solution (0.2 mol L^{-1}) was added, and the mixture was shaken for 1 min to uniformly mix $CaCl_2$ and blood. The prepared samples were placed in the constant temperature bath at 37 °C for 10, 30, 50, and 70 min. A volume of 50 mL of distilled water was added and shaken for 10 min. At last the supernatant was centrifuged to measure the optical density of the sample at a wavelength of 540 nm by a spectrophotometer (UV-2600, Shimadzu, Japan). Distilled water was used as a reference control, in which 50 mL of the solution contained 0.25 mL of whole blood, and the same experimental method was used to perform a blank experiment without a membrane. Six groups were measured in parallel and averaged.

Cytotoxicity test

According to the requirement of ISO 10993, the electrospun membranes were irradiated by Co-60 rays at 2 kGy h^{-1} intensity for 10 h, and then placed in a RPMI 1640 medium and incubated at 37 °C for 24 h to get the original liquid of sample PLCL and 8 wt% TM NPs/PLCL. Subsequently, a certain volume of extract was taken and diluted with culture medium

to prepare 25%, 50% and 75% diluents. 2×10^3 fibroblast L929 was inoculated into a 96-well plate and cultured for 24 h at 37 °C and 5% CO_2 to ensure adherence. Then the supernatant of the cell culture plate was removed and 200 μL of extracted solution or the leaching diluent (three compound holes for each test sample) was added to cultivate for 72 h in the incubator.

Finally, 10 μL per well of MTT (5 mg mL^{-1}) was added into the cell culture plate, and incubated at 37 °C for 4 h, after which the supernatant was removed and 180 μL DMSO was added. The optical density of each sample at a wavelength of 570 nm was measured by an enzyme-labeled instrument (Multiskan FC, Thermo Scientific, USA).

Cell morphology

The TM NPs/PLCL membranes were irradiated by Co-60 rays at 2 kGy h^{-1} intensity for 10 h. 2×10^4 L929 cells were seeded per well in a 24-well plate and cultured for 72 h. The cells were fixed by 2% glutaraldehyde and 2% paraformaldehyde in PBS at 4 °C for 4 h, dehydrated with 60%, 70%, 80%, 90%, 100% absolute ethanol solution, and freeze-dried for 24 h. The dried sample was subjected to gold spray treatment and the surface morphology was observed at an accelerating voltage of 5 kV using a scanning electron microscope (SEM, S4800, Hitachi, Japan).

Mechanical properties

Samples having 7 cm length and 1 cm width were prepared in accordance with the ISO 527-3:1995 standard. The tensile strength, elongation at break and Young's modulus of different samples were measured using an Electromechanical Universal Testing Machine (T6104, Shenzhen Sans Testing Machine Co., Ltd. PRC) with an inlet force of 0.5 N and a tensile speed of 10.0 mm min^{-1}.

Statistical analysis

The data were represented as the mean ± standard error and compared by using one-way ANOVA tests. A p-value less than 0.05 was considered as a statistically significant difference between pairs.

Table 1 The viscosity, conductivity and surface tension of electrospinning solution for different samples

Samples	Viscosity (cP)	Conductivity (μS cm^{-1})	Surface tension (mN m^{-1})
PLCL	79.80	4.67	29.63
2% TM NPs/PLCL	103.50	6.88	29.35
4% TM NPs/PLCL	142.20	9.21	29.20
6% TM NPs/PLCL	180.80	10.82	29.09
8% TM NPs/PLCL	230.40	12.36	29.22

Results and discussion

High-magnification SEM image (Fig. 1a) showed that the processed tourmaline nanoparticles were mainly spherical and ellipsoidal, and the diameters of most particles were less than 100 nm. The XRD patterns of TM NPs were in accordance with TM (Fig. 1b). Zeta potential indicated the surface charge density of dispersed particles in solution. Fig. 1c shows that the zeta potential of the tourmaline nanoparticles/ethanol system and the tourmaline ore/ethanol system were −15.2 mV and −5.78 mV, respectively, which showed that tourmaline nanoparticles have a higher surface charge density.

The viscosity, electrical conductivity and surface tension of the TM NPs/PLCL electrospinning solution are shown in Table 1. As the tourmaline content increased, the viscosity of the electrospinning solution increased from 79.80 cP to 230.40 cP and the conductivity of the electrospinning solution increased from 4.67 μS cm^{-1} to 12.36 μS cm^{-1}, while the surface tension of the solution did not change significantly. The increase in solution viscosity was attributed to the surface effect of TM NPs capable of adsorbing the polymer chain in the electrospinning solution,[26,27] which transmits its own excessive energy, hindering the movement of the segments to enhance the entanglement between the polymer segments. In addition, each of the tourmaline nanoparticles in the solution were equivalent to an electric dipole due to its spontaneous polarization effect,[28] which led to the increase in the conductivity of the whole solution.

Fig. 2 displays the SEM patterns for the PLCL and composite membranes. The electrospun membrane was composed of a large number of randomly oriented fibers, which were interconnected to create a three-dimensional porous network

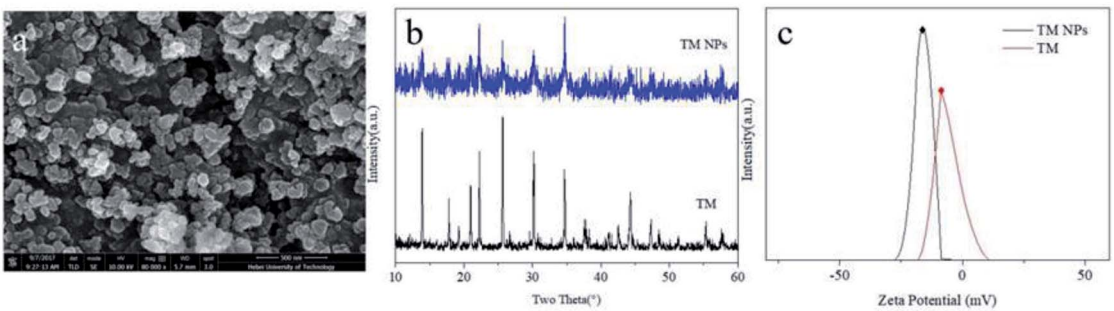

Fig. 1 Surface morphology (a), XRD (b) and zeta potential (c) of TM NPs.

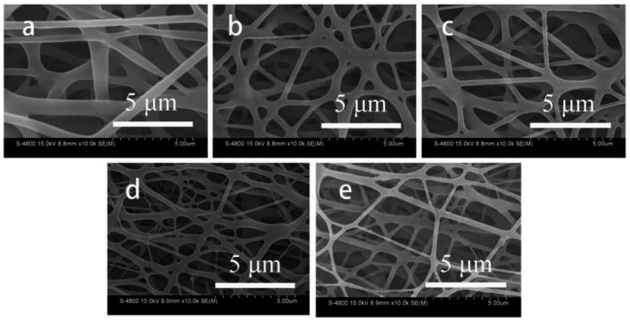

Fig. 2 SEM images of different electrospun membranes ((a) PLCL, (b) 2 wt% TM NPs/PLCL, (c) 4 wt% TM NPs/PLCL, (d) 6 wt% TM NPs/PLCL, (e) 8 wt% TM NPs/PLCL).

structure. The morphology of the electrospun fibers was not affected by the introduction of tourmaline nanoparticles. All the electrospun membranes consist of uniform ultrafine fibers. Using Image J, the average diameter of the electrospun fibers fall in the range from 751.7 ± 324.3 nm (PLCL) to 532.4 ± 372.8 nm (8 wt% TM NPs/PLCL). This was attributed to the charging jet that does not break up into small droplets due to chain entanglements of higher viscosity, thereby allowing the coulombic stress to elongate the charged jet to form into thinner fibers. Furthermore, because of the highly conductive solution, the fiber jet would get more stretched by the electric field force, causing the diameter of the fiber to be reduced.

Fig. 3 shows the TEM images of the PLCL and TM NPs/PLCL nanofibers containing 2 wt%, 4 wt%, 6 wt% and 8 wt% TM NPs. It is found that the PLCL sample displayed smooth and cylindrical fibers. Additionally, the TM NPs can be dispersed in the PLCL fiber without a dispersant because the high surface charge density of TM NPs causes electrostatic repulsion among them, which contributes to their dispersion in PLCL solution.[29] Therefore, the uniform dispersion was directly related to the increase in TM NP contents in the composite solution and spun fibers. Additionally, the crystal structure of TM NPs in 8 wt% TM NPs/PLCL was detected (ESI Fig. S2†), which was consistent with XRD characterization (Fig. 1b).

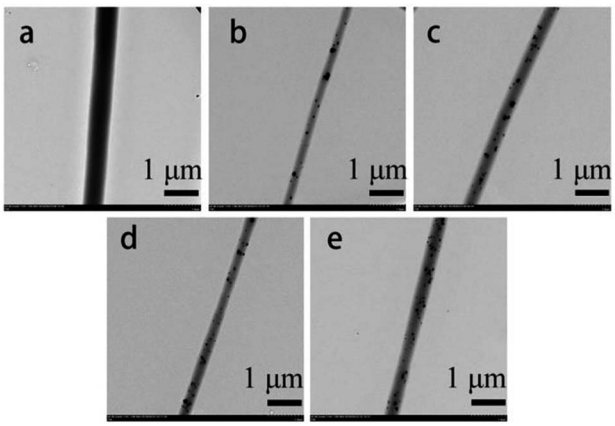

Fig. 3 TEM images of different electrospun membranes ((a) PLCL, (b) 2 wt% TM NPs/PLCL, (c) 4 wt% TM NPs/PLCL, (d) 6 wt% TM NPs/PLCL, (e) 8 wt% TM NPs/PLCL).

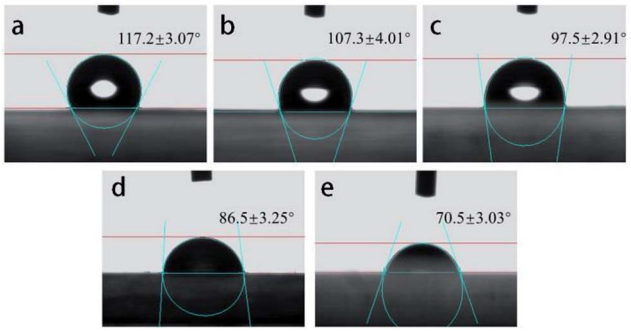

Fig. 4 Contact angle of different electrospun membranes ((a) PLCL, (b) 2 wt% TM NPs/PLCL, (c) 4 wt% TM NPs/PLCL, (d) 6 wt% TM NPs/PLCL, (e) 8 wt% TM NPs/PLCL).

The wettability of the samples could be evaluated by the contact angle (Fig. 4). It was clear that the contact angle of the membranes decreased with the loading of TM NPs into the fibers. When the tourmaline nanoparticle content was 8 wt%, the contact angle was 70.5 ± 3.7°, which was 47° lower than that of the PLCL membrane (117.2 ± 3.1°). This decrease was directly attributed to the better hydrophilicity of TM. Moreover, hydrogen bonds in water clusters were destroyed by the electric field of TM NPs.[20,21] Therefore, the surface tension of water was reduced, and the hydrophilicity of composite membrane was improved.

Blood clotting measurements were often used to assess the influence of materials on the process of the intrinsic coagulation pathway. When the membranes come in contact with blood, intrinsic coagulation occurrs and the degree of coagulation increases following the contact time (Fig. 5). The optical density curves reflected the trend of the number of free hemoglobin in the blood supernatant. Generally, the optical density value equal to 0.1 was taken as the initial clotting time. The values of the control and the samples except 8 wt% TM NPs/PLCL exhibited a similar rapidly decreasing profile. The initial clotting time of the control, PLCL, 2 wt% TM NPs/PLCL, 4 wt% TM NPs/PLCL and 6 wt% TM NPs/PLCL samples were 41.1 min, 41.9 min, 43.1 min, 44 min and 45 min, respectively. The clotting time of the 8 wt% TM NPs/PLCL sample was more

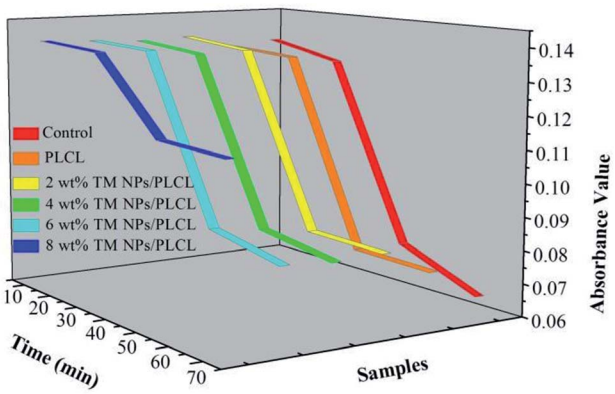

Fig. 5 Anticoagulant properties of different electrospun membranes.

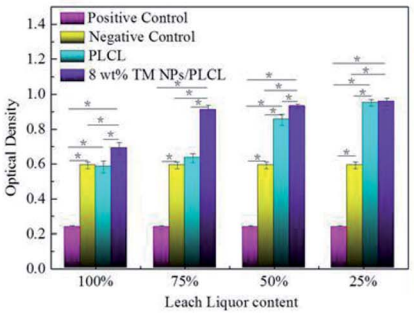

Samples	Leach Liquor content	RGR	Toxicity Grade
Negative Control	——	——	——
Positive Control	——	39.81%	3
PLCL	100%	98.53%	1
8 wt%TM NPs/PLCL		116.53%	0
PLCL	75%	107.05%	0
8 wt%TM NPs/PLCL		153.91%	0
PLCL	50%	144.24%	0
8 wt%TM NPs/PLCL		157.21%	0
PLCL	25%	160.61%	0
8 wt%TM NPs/PLCL		161.88%	0

Fig. 6 Cytotoxicity of different samples (PLCL, 8 wt% TM NPs/PLCL, positive control and negative control).

than 70 min, which was much longer than the other samples. These data indicated that the composite membranes with TM NP additives reduced the activation of intrinsic clotting factors in the blood and prolonged the dynamic clotting time.

From the existing literatures, it was believed that TM NPs could improve the anticoagulant properties of the materials by the following three aspects. First, the diameter of electrospun fibers was reduced by adding TM NPs, thus a smoother membrane surface was constructed, which reduced the blood flow resistance. Second, the hydrophilicity of the composite membrane was improved, which could hinder protein adhesion. Finally, the negative potential of TM NPs led to the electrostatic repulsion of platelets, which reduced the possibility of platelets sticking to the membrane surface.

Cytotoxicity tests were also carried out to determine whether the composite membrane had the potential to act as a small-caliber vascular graft. The MTT assay was based on the reaction between MTT and mitochondrial succinate dehydrogenases in living cells to form a purple formazan, which was soluble in DMSO but insoluble in water. The OD value of the formazan–DMSO solution was considered to be proportional to the number of living cells. Therefore, it was often used to evaluate cytotoxicity. After 3 days of treatment, the optical density of L929 cells on the negative control, positive control, PLCL and 8 wt% TM NPs/PLCL membranes are shown in Fig. 6. In the positive control group, the RGR of L929 is 39.81%, the cytotoxicity grade is 3, which is moderately cytotoxic. For 100% extracts of samples, the RGR of 8 wt% TM NPs/PLCL (116.53%) was 1.18 times that of the RGR of PLCL (98.53%), showing the positive effect on cell proliferation following tourmaline addition. Besides, the cytotoxicity grade of PLCL and 8 wt% TM NPs/PLCL membrane were 1 and 0, respectively. For other percent extracts, the RGR of L929 cells on PLCL and 8 wt% TM NPs/PLCL membranes increased with decreasing extract concentration, and the cytotoxicity grade of both PLCL and 8 wt% TM NPs/PLCL membranes was 0. Compared with the positive control group and negative control group, the two samples showed no toxicity and had potential application in biological systems.

Fig. 7 displays the SEM patterns for L929 cells on the control, PLCL and 8 wt% TM NPs/PLCL membranes. In the control group, L929 cells were fusiform, solitary and had distinct pseudopods. In the PLCL group, the L929 cells were spindle-shaped and polygonal. In the 8 wt% TM/PLCL group, L929 cells were also fusiform or polygonal. However, unlike the control group, the cells grew continuously and the number of cells was more than the control group. In addition, the pseudopods were mainly covered by electrospun fibers and had a tendency to grow into the membrane.

Fig. 8 shows the tensile strength and elongation at the break of different TM NPs/PLCL composite membranes. The tensile strength increased from 2.51 ± 0.25 MPa to 6.71 ± 0.30 MPa with the increase in TM NPs content, which meant that the tensile strength increased by 267.33% on the PLCL membrane. This enhancement was attributed to the following points: first, the added TM NPs provided a nucleation particle for the polymer solution during electrospinning, which helped to improve the crystallinity of the composite (confirmed through DSC, Fig. S3 in ESI†). Secondly, the unique surface and small size effect of the nano-size could impact the physical and chemical

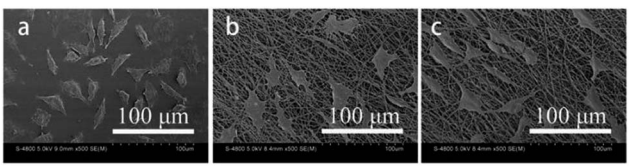

Fig. 7 Cell morphologies of L929 cultured on different membranes (control, PLCL and 8 wt% TM NPs/PLCL).

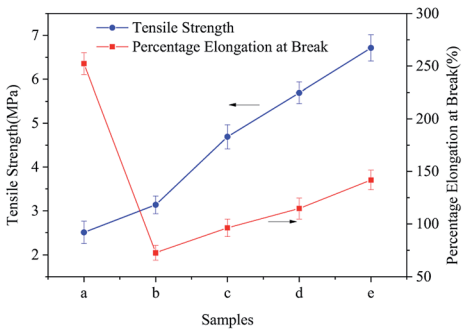

Fig. 8 Mechanical properties of different electrospun membranes ((a) PLCL, (b) 2 wt% TM NPs/PLCL, (c) 4 wt% TM NPs/PLCL, (d) 6 wt% TM NPs/PLCL, (e) 8 wt% TM NPs/PLCL).

interaction between uniformly distributed nanoparticles.[29] When the substrate was subjected to an external force, the entanglement point inhibited the sliding of the molecular chain.[30] Finally, nanoparticles could also act as stress concentration points to prevent further cracking.[31]

The elongation at the break of the composite membrane showed a trend of fall-rise, when the TM NPs content was 2 wt%, the elongation at break of the composite film was the lowest (72.65 ± 6.85%), which could not meet the requirement for the coronary artery (99%).[32] The composite membrane containing 6 wt% or 8 wt% of TM NPs had good toughness with an elongation at break of more than 100%. The introduction of TM NPs aggravated the brittleness of fibers, causing a decrease in the elongation at break. However, with the increase in TM NPs content, the incorporation could not only transmit the external stress, but also cause the matrix yielding to consume a large amount of energy, thus achieving the toughening of the composite membranes.

Conclusions

In this study, TM NPs/PLCL membranes with good dispersion were obtained by reducing the diameter of tourmaline and improving the preparation method of electrospun solutions without adding a dispersant. Subsequently, dynamic coagulation experiments verified our assumption that the addition of tourmaline could improve the anticoagulant properties of the electrospun PLCL matrix. The OD value of 8 wt% TM NPs/PLCL membrane was 0.113 when it was in contact with anticoagulant rabbit blood for 70 minutes, which was 174% higher than that of PLCL. At the same time, cytotoxicity tests showed that the grade of 8 wt% TM NPs/PLCL membrane was 0, which meant TM NPs had no cytotoxicity to fibroblast. The stretching experiment results showed that the 8 wt% TM NPs/PLCL composite membrane had good mechanical properties. The tensile strength of 8 wt% TM NPs/PLCL membrane (6.71 ± 0.30 MPa) was 267.33% higher than that of PLCL membrane, and the elongation at break (141.83 ± 5.82%) was higher than the requirement of the coronary artery. These experiments explored the possibility of TM NPs/PLCL electrospun membranes being used in tissue engineering as small-caliber vascular grafts. Further investigation will be conducted in our subsequent research.

Conflicts of interest

There are no conflicts to declare.

Acknowledgements

This project was supported by the National Natural Science Foundation of China (Grant No. 51504076) and the Natural Science Foundation of Hebei Province of China (Grant No. E2016202379).

References

1 M. A. Cleary, E. Geiger, C. Grady, C. Best, Y. Naito and C. Breuer, *Trends Mol. Med.*, 2012, **18**, 394–404.
2 A. Pangesty and M. Todo, *Mater. Lett.*, 2018, **228**, 334–338.
3 F. Gaertner and S. Massberg, *Semin. Immunol.*, 2016, **28**, 561–569.
4 L. Eyre and F. Gamlin, *Anaesthesiol. Intensive Care Med.*, 2010, **11**, 244–246.
5 O. N. Okafor and D. A. Gorog, *J. Am. Coll. Cardiol.*, 2015, **65**, 1683–1699.
6 A. T. Long, E. Kenne, R. Jung, T. A. Fuchs and T. Renné, *J. Thromb. Haemostasis*, 2016, **14**, 427–437.
7 M. Rabe, D. Verdes and S. Seeger, *Adv. Colloid Interface Sci.*, 2011, **162**, 87–106.
8 J. Gao, Y. Wang, S. Chen, D. Tang, L. Jiang, D. Kong and S. Wang, *RSC Adv.*, 2017, **7**, 18775–18784.
9 X. Li, J. Tang, L. Bao, L. Chen and F. F. Hong, *Carbohydr. Polym.*, 2017, **178**, 394–405.
10 M. Lovett, C. Cannizzaro, L. Daheron, B. Messmer, G. Vunjak-Novakovice and D. L. Kaplan, *Biomaterials*, 2007, **28**, 5271–5279.
11 D. Ma, Y. Wang and W. Dai, *Mater. Sci. Eng., C*, 2018, **89**, 456–469.
12 A. Maslow, A. Chambers, T. Cheves and J. Sweeney, *J. Cardiothorac. Vasc. Anesth.*, 2018, **32**, 1603–1608.
13 M. Erginer, A. Akcay, B. Coskunkan, T. Morova, D. Rende, S. Bucak, N. Baysal, R. Ozisik, M. S. Eroglu, M. Agirbasli and E. Toksoy Oner, *Carbohydr. Polym.*, 2016, **149**, 289–296.
14 A. K. A. Silva, M. Juenet, A. Meddahi-Pellé and D. Letourneur, *Carbohydr. Polym.*, 2015, **116**, 267–277.
15 P. Xiang, S. Wang, M. He, Y. Han, Z. Zhou, D. Chen, M. Li and L. Q. Ma, *Colloids Surf., B*, 2018, **163**, 19–28.
16 H. Zhang, X. Jia, F. Han, J. Zhao, Y. Zhao, Y. Fan and X. Yuan, *Biomaterials*, 2013, **34**, 2202–2212.
17 H. Guo, W. Dai, D. Qian, Z. Qin, Y. Lei, X. Hou and C. Wen, *Acta Biomater.*, 2017, **54**, 107–116.
18 Y. Hu, X. Pan, J. Zheng, W. Ma and L. Sun, *Int. J. Surg.*, 2017, **44**, 244–249.
19 F. Zhou, M. Wen, P. Zhou, Y. Zhao, X. Jia, Y. Fan and X. Yuan, *Mater. Sci. Eng., C*, 2018, **85**, 37–46.
20 Y. Song, D. Zhu, J. Liang and X. Zhang, *Ceram. Int.*, 2018, **44**, 15550–15556.
21 H. Zhang, A. Lv, J. Liang and J. Meng, *RSC Adv.*, 2015, **5**, 55704–55712.
22 H. Zhang, P. Li, N. Hui and J. Liang, *J. Controlled Release*, 2017, **259**, e44–e45, DOI: 10.1016/j.jconrel.2017.03.113.
23 A. De Mori, M. Peña Fernández, G. Blunn, G. Tozzi and M. Roldo, *Polymers*, 2018, **10**, 285.
24 H. Zhang, J. Liang, Y. Ding and P. Li, *Mater. Lett.*, 2016, **181**, 119–122.
25 L. D. Tijing, M. T. G. Ruelo, A. Amarjargal, H. R. Pant, C.-H. Park, D. W. Kim and C. S. Kim, *Chem. Eng. J.*, 2012, **197**, 41–48.
26 D. Wu, L. Wu and M. Zhang, *J. Polym. Sci., Part B: Polym. Phys.*, 2007, **45**, 2239–2251.

27 Y. Bai, X. Shang, Z. Wang and X. Zhao, *Colloids Surf., A*, 2018, **551**, 95–107.
28 P. Rajeshwari and T. K. Dey, *Mater. Chem. Phys.*, 2017, **190**, 175–186.
29 M. Shoyama, T. Kawata, M. Yasuda and S. Matsusaka, *Adv. Powder Technol.*, 2018, **29**, 1960–1967.
30 R. K. Nayak and B. C. Ray, *Arch. Civil Mech. Eng.*, 2018, **18**, 1597–1607.
31 Y. Hu, G. Du and N. Chen, *Compos. Sci. Technol.*, 2016, **124**, 36–43.
32 W. He, T. Yong, W. Ten, W. E. Teo, Z. Ma and S. Ramakrishna, *Tissue Eng.*, 2005, **11**, 1574–1588.